Absence of strong magnetic fluctuations or interactions in the normal state of $LaNiGa_2$

P. Sherpa,[1] I. Vinograd,[1] Y. Shi,[1] S. A. Sreedhar,[1] C. Chaffey,[1] T. Kissikov,[1] M.-C. Jung,[2] A. S. Botana,[2] A. P. Dioguardi,[3] R. Yamamoto,[3] M. Hirata,[3] G. Conti,[4] S. Nemsak,[4] J. R. Badger,[5] P. Klavins,[1] I. Vishik,[1] V. Taufour,[1] and N. J. Curro[1]

[1]*Department of Physics and Astronomy, University of California, Davis, California 95616, USA*
[2]*Department of Physics, Arizona State University, Tempe, AZ 85287, USA*
[3]*Los Alamos National Laboratory, Los Alamos, New Mexico 87545, USA*
[4]*Advanced Light Source, Lawrence Berkeley National Laboratory, Berkeley, California, 94720, USA*
[5]*Department of Chemistry, University of California, Davis, California 95616, USA*

(Dated: February 2, 2024)

We present nuclear magnetic (NMR) and quadrupole (NQR) resonance and magnetization data in the normal state of the topological crystalline superconductor $LaNiGa_2$. We find no evidence of significant magnetic fluctuations or enhanced paramagnetism. These results suggest that the time-reversal symmetry breaking previously reported in the superconducting state of this material is not driven by strong electron correlations.

I. INTRODUCTION

The emergence of unconventional superconductivity is generally accepted to be a consequence of electron-electron interactions in materials that usually exhibit strong magnetic correlations in the normal state [1]. These correlations can also play an important role in the behavior of the class of unconventional superconductors that break time-reversal symmetry (TRS) in the superconducting state. This property reveals important information about the nature of the superconducting condensate, such as triplet pairing, or if there are multiple components of the superconducting order parameter [2–5]. The vast majority of superconductors do not exhibit TRS breaking, however those that do may have nontrivial topological properties that could support Majorana zero modes, which potentially could be exploited as dissipationless qubits for quantum computing [6, 7]. Determining the presence and origin of TRS breaking in the superconducting state is challenging, because the associated magnetic field is typically very small and is usually detected only via muon spin relaxation (μSR) [8, 9] or polar Kerr effects [10].

The intermetallic superconductor $LaNiGa_2$ has recently attracted attention because μSR experiments in this material uncovered TRS breaking in the superconducting state below $T_c = 2.1$ K [11]. This material has a similar stoichiometry as $LaNiC_2$ [12], which also exhibits TRS breaking due to a combination of spin-orbit coupling and a non-centrosymmetric structure [13]. However, $LaNiGa_2$ is centrosymmetric and recent penetration depth, specific heat, and μSR measurements have revealed multiple, nodeless gaps [14–16]. A recent single crystal study revealed that $LaNiGa_2$ actually has a nonsymmorphic crystal structure that gives rise to a nontrivial band topology [17] with band-degeneracies at the Fermi level. This electronic structure can support interband pairing and a superconducting order parameter that can be antisymmetric in the band channel, allowing for fully-gapped equal-spin pairs.

An important open question is what drives the imbalance between two equal-spin gaps resulting in the time-reversal symmetry breaking that was observed below T_c [11]. Non-unitary multiorbital superconductivity may arise from competing interactions [18], and spin fluctuations are generally present in the normal state of unconventional superconductors [1, 19]. It is therefore important to investigate the strength of electron correlations that may be present in the normal state of $LaNiGa_2$. Here we report nuclear magnetic resonance (NMR), nuclear quadrupole resonance (NQR), bulk magnetization, and X-ray photoelectron spectroscopy (XPS) measurements, as well as density-functional theory (DFT) calculations, that reveal the absence of any significant spin fluctuations or Stoner enhancement, suggesting that electron correlation effects in this material are weak and therefore unlikely to play a role in the unusual superconducting pairing.

II. METHODS

Single crystals of $LaNiGa_2$ were grown via flux methods as described in [17]. This material has one La site and two crystallographically distinct Ga sites [dubbed Ga(1) and Ga(2) hereafter], as illustrated in Fig. 1(a). Magnetization measurements were performed with a Magnetic Property Measurement System (MPMS, Quantum Design) in the temperature range of 2 K to 300 K. Because the magnetic susceptibility is relatively small, we prepared a mosaic of co-aligned single crystals, allowing for a larger signal.

XPS measurements were performed using a lab-based XPS setup (Kratos Axis Supra). The Ga $2p_{3/2}$ core levels were obtained using an Al K-α source and Ag L-α on the single crystals at room temperature.

For the NMR measurements, three single crystals were aligned to make a mosaic with dimensions $1.3 \times 0.5 \times 0.5$ mm^3, secured in an coil, and placed in an external field in a cryostat. The resonance frequencies are determined

by the Hamiltonian:

$$\mathcal{H} = \gamma\hbar\hat{\mathbf{I}}\cdot(1+\mathbf{K})\cdot\mathbf{H}_0 + \frac{h\nu_{zz}}{6}\left[3\hat{I}_z^2 - \hat{I}^2 + \eta(\hat{I}_x^2 - \hat{I}_y^2)\right] \quad (1)$$

where γ is the gyromagnetic ratio, h ($\hbar$) is the Planck (reduced Planck) constant, $\hat{\mathbf{I}}$ is the nuclear spin angular momentum operator, $\mathbf{H}_0$ is the external magnetic field vector, $\mathbf{K}$ is the NMR shift tensor, $\eta = (\nu_{xx} - \nu_{yy})/\nu_{zz}$ is the asymmetry parameter, and $\nu_{\alpha\alpha} = 3eQV_{\alpha\alpha}/2I(2I-1)h$ are the principal values of the electric field gradient (EFG) tensor, $V_{\alpha\beta}$, (where α and β stand for one of the three directions of the principal axes of the EFG tensor), I is the nuclear spin quantum number, and Q is the nuclear quadrupolar moment. The NMR parameters for each isotope is given in Table I. NMR spectra were measured by integrating the echo intensity as a function of frequency in either a field of $\mu_0 H_0 = 11.7286$ T or 7.0 T at 5 K for fields both parallel and perpendicular to the b-axis. The Knight shift and EFG components, $K_{\alpha\alpha}$ and $\nu_{\alpha\alpha}$, were determined by fitting the full spectra to exact diagonalization results for Eq. 1 for various orientations of $\mathbf{H}_0$. NQR spectra were acquired at zero applied field at 4 K by integrating the Fourier transform of the echo intensity as a function of frequency.

The spin-lattice relaxation rate, T_1^{-1}, was measured by NMR using the inversion recovery method at the central transition ($I_z = +1/2 \leftrightarrow -1/2$) of ^{139}La and ^{69}Ga(1) sites as a function of temperature in a magnetic field of 7 T. The recovery of nuclear magnetization after inversion for the ^{139}La site was fitted to the standard expression for a nuclear spin $I = 7/2$ system: $M(t) = M_0\left(1 - 2f\sum_n A_n e^{-\alpha_n t/T_1}\right)$, where M_0 is the equilibrium nuclear magnetization, f is the inversion fraction, $A_1 = 1225/1716$, $A_2 = 75/364$, $A_3 = 3/44$, $A_4 = 1/84$, $\alpha_1 = 28$, $\alpha_2 = 15$, $\alpha_3 = 6$, and $\alpha_4 = 1$. For the ^{69}Ga(1) site with a nuclear spin $I = 3/2$, the recovery was fitted using $A_1 = 9/10$, $A_2 = 1/10$, $\alpha_1 = 6$, and $\alpha_2 = 1$.

We performed density-functional theory (DFT)-based calculations for $LaNiGa_2$ using the all-electron full-potential code, Wien2k [20]. The exchange-correlation functional used was the Perdew-Burke-Erznerhof version of the generalized gradient approximation (PBE-GGA) [21]. The number of plane waves was limited by a cut-off set by $R_{mt}K_{max} = 7$ and the muffin-tin radii used were 2.5 a.u. for La, 2.32 a.u. for Ni, and 2.20 a.u. for Ga the atoms. In order to obtain the EFG tensors, we used a very fine k-mesh of $34 \times 34 \times 33$ in the irreducible Brillouin zone.

TABLE I. NMR parameters for the three isotopes measured in $LaNiGa_2$.

isotope	^{139}La	^{69}Ga	^{71}Ga
abundance	99.1%	60%	40%
I	7/2	3/2	3/2
$\gamma/2\pi$ (MHz/T)	6.0146	10.219	12.985
Q (barn)	0.21	0.178	0.112

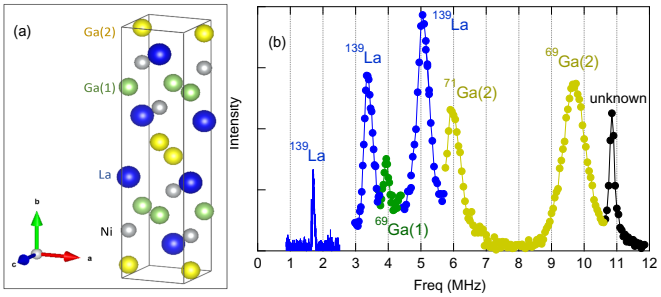

FIG. 1. (a) Unit cell of $LaNiGa_2$. (b) NQR spectrum measured at 4 K of a powdered sample. The ^{71}Ga(1) resonance near 2.5 MHz is not shown.

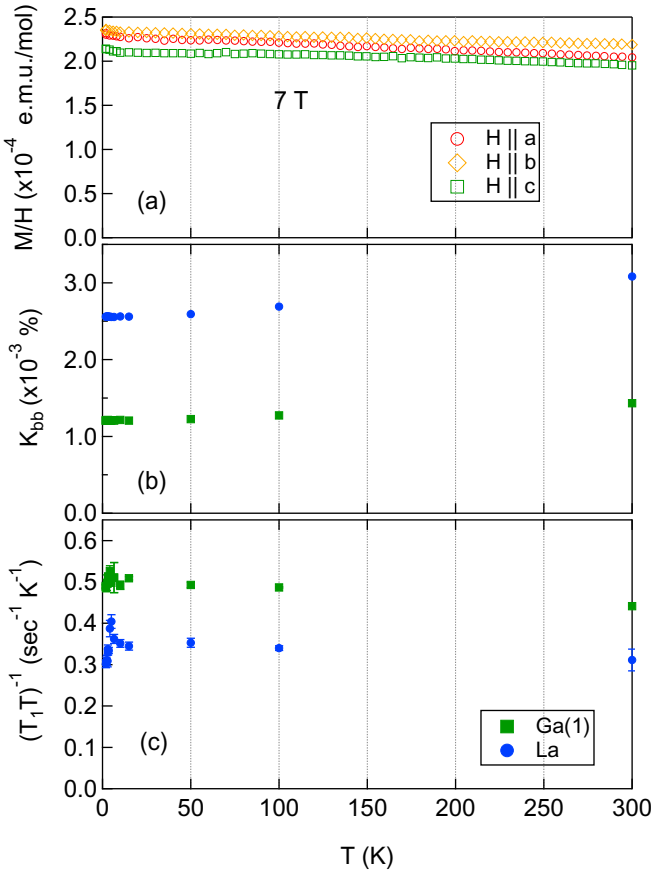

FIG. 2. (a) Susceptibility as a function of temperature of an aligned mosaic of single crystals of $LaNiGa_2$ with the magnetic field along the a, b and c axes. (b) The Knight shift K and (c) the spin-lattice relaxation rate divided by temperature $(T_1T)^{-1}$ plotted against temperature for both the ^{139}La and ^{69}Ga(1) sites for the field along the b axis.

III. RESULTS

A. Stoner enhancement factor

Figure 2(a) shows the DC magnetic susceptibility of a mosaic of $LaNiGa_2$ single crystals with an applied magnetic field of 7 T along the a, b and c axes. The susceptibility appears to be almost temperature-independent, suggesting Pauli paramagnetic behavior. By averaging the susceptibility values across the entire temperature range, we obtain susceptibilities of 2.17×10^{-4}, 2.26×10^{-4} and 2.05×10^{-4} e.m.u./mol along the a, b and c axes, respectively.

In general, the measured temperature-independent susceptibility χ_{meas} consists of two components: the paramagnetic contribution from conduction electrons, χ_P, and the diamagnetic contribution, χ_D, from the atomic cores. According to DFT calculations, the Ni $3d$ band is filled [29]. We therefore can estimate the Langevin diamagnetic susceptibility of $Ni^{3d^{10}}$ by extrapolating from that of other ions with the same $3d$ electron configuration, such as Cu^+, Zn^{2+}, Ga^{3+}, and Ge^{4+} [30]. This gives a value of $\chi_{D,Ni^{3d^{10}}} = -19 \times 10^{-6}$ e.m.u./mol. For the La site we use $\chi_{D,La^{3+}} = -20 \times 10^{-6}$ e.m.u./mol [31].

In order to determine the diamagnetic contribution from the Ga, we first performed XPS to determine the Ga electronic configuration. Figure A1 in the appendix shows sub-peaks corresponding to neutral Ga(0) (BE=1116.4 eV) [32, 33] and Ga(III) (BE= 1117.8 eV) [32, 33]. The Ga(III) peak shows significant attenuation between freshly cleaved (Fig. A1(b)) and air-exposed samples (Fig. A1(a)) with the binding energy matching well with literature values for Ga_2O_3 [32, 33]. This observation agrees with the species being a surface oxide as seen by changing to a Ag L-α source (Fig. A1(c)) wherein the relative ratio of the peaks changes to be more bulk dominated [34]. We conclude that the bulk oxidation state of Ga is neutral, therefore $\chi_{D,Ga^0} = -32 \times 10^{-6}$ e.m.u./mol [30]. This yields a total diamagnetic susceptibility $\chi_D = -10.3 \times 10^{-5}$ e.m.u./mol for $LaNiGa_2$.

The Pauli susceptibility of a free electron gas is given by $\chi_P = \left(3\mu_0\mu_B^2 10^6/4\pi^3 k_B^2\right)\gamma_S$, where γ_S is the Sommerfeld coefficient. Using $\gamma_S = 14.1\,\mathrm{mJ{\cdot}mol^{-1}{\cdot}K^{-2}}$ [17], we obtain $\chi_P = 1.93 \times 10^{-4}$ e.m.u./mol. Using the values for χ_P and χ_D, we can now extract the Stoner enhancement factor, Z, from the measured susceptibility via the relation:

$$\frac{1}{1-Z} = \frac{\chi_{meas} - \chi_D}{\chi_P}. \tag{2}$$

We find $Z = 0.40$, 0.41, and 0.37 along the a, b, and c axes respectively. These Z values are smaller than the Stoner limit ($Z = 1$) and comparable with the estimated value of copper, $Z = 0.26$ (using γ_S=0.505 $\mathrm{mJ{\cdot}mol^{-1}{\cdot}K^{-2}}$ [35] and $\chi_0 = -14.85 \times 10^{-6}$ e.m.u./mol [30]). These results thus indicate that there is no significant enhancement of the paramagnetic susceptibility due to ferromagnetic interactions.

B. Magnetic Resonance

1. *Electric Field Gradient*

Fig. 1(b) shows the NQR spectrum measured at 4 K. There are several peaks, and it is not obvious a priori which transitions correspond to which site. In an applied field the ^{139}La NMR spectrum (Fig. B1 in the appendix) reveals seven transitions at frequencies split by $\nu_{\alpha\alpha}$. These splittings enable us to identify the EFG at the La site and hence the three peaks in blue shown in the NQR spectrum. The fitted values of the tensor elements are given in Table. II. The EFG vector (the direction corresponding to the largest eigenvalue of the EFG tensor) lies along the b-direction. However, the EFG asymmetry paramter is remarkably small: $\eta = 0.04 \pm 0.01$. This indicates that the three La peaks in Fig. 1(b) approximately correspond to the three transitions of $I_z = \pm 1/2 \leftrightarrow \pm 3/2$, $I_z = \pm 3/2 \leftrightarrow \pm 5/2$, and $I_z = \pm 5/2 \leftrightarrow \pm 7/2$ from low to high frequency peaks. The NQR frequency of the La is similar to that observed in $LaNiC_2$, which has a similar structure but is non-centrosymmetric [36].

The remaining resonances in the NQR spectrum are due to the transition of $I_z = \pm 1/2 \leftrightarrow \pm 3/2$ at the two Ga sites in the unit cell [Ga(1) and Ga(2) in Fig.1(a)], which each have two spin 3/2 isotopes (^{69}Ga and ^{71}Ga), giving us in total four transition peaks. To identify the EFG at these sites, we performed NMR in an applied field as a function of angle, as discussed in the appendix. The fitted values of the EFG are given in Table II. There is a large asymmetry parameter η for both sites, reflecting the orthorhombic nature of the local electronic environment. The EFG vector for one of the two Ga sites lies along the b-axis, similar to the La site, however for the other site the EFG vector lies along the c-axis.

In order to discern the transitions for the two different sites and two isotopes, we turn to the DFT calculations, whose values are given in Table II. For both the La and Ga(1) sites, the EFG vector lies along the b-axis, but for the Ga(2) site it lies along the c-axis, enabling us to assign the two Ga resonances. We find that the lower frequency peak with $^{69}\nu_Q = 3.94 \pm 0.01$ MHz corresponds to the Ga(1) site, and the higher frequency peak with $^{69}\nu_Q = 9.70 \pm 0.01$ MHz corresponds to the Ga(2) site. The observed and theoretical values are within 20% of each other.

The NQR spectrum in Fig. 1(b) also reveals a smaller third resonance near 11 MHz. The origin of this third resonance is unknown, although the NQR frequency is close to that of pure ^{69}Ga metal [37]. It may also arise from an impurity phase, such as LaNiGa which is close to the composition of the flux and has been detected in

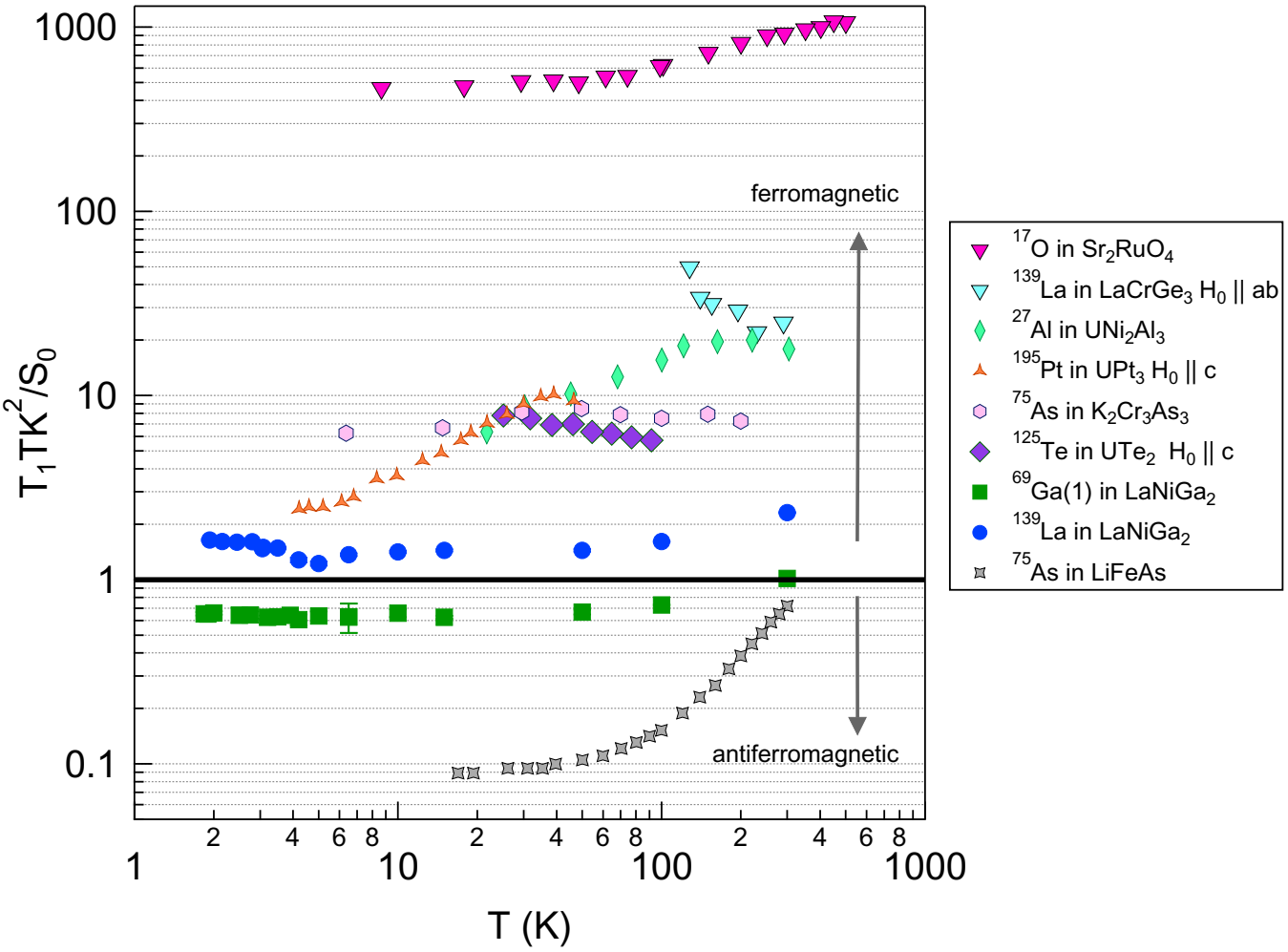

FIG. 3. The Korringa ratio, T_1TK^2/S_0, versus temperature for $LaNiGa_2$ (for field along the b direction) compared with data for LiFeAs [22], UTe_2 [23], UNi_2Al_3 [24], $LaCrGe_3$ [25], $K_2Cr_3As_3$ [26], UPt_3 [27], and Sr_2RuO_4 [28].

TABLE II. EFG parameters for the Ga(1), Ga(2) and La sites in $LaNiGa_2$ determined from NQR and NMR spectra. (a, b, c) correspond to the unit cell axes shown in Fig. B1(a). ν_Q is defined as $\nu_{zz}\sqrt{1+\eta^2/3}$, where ν_{zz} is the largest eigenvalue. Computed values are from band structure calculations as described in the text.

site	ν_{aa} (MHz)	ν_{bb} (MHz)	ν_{cc} (MHz)	ν_Q (MHz)	η
Ga(1) measured	-2.61 ± 0.01	3.86 ± 0.01	-1.25 ± 0.01	3.94 ± 0.01	0.35 ± 0.01
Ga(1) computed	-1.091	4.332	-3.241	4.506	0.496
Ga(2) measured	-0.78 ± 0.01	-7.99 ± 0.01	8.77 ± 0.01	9.70 ± 0.01	0.82 ± 0.01
Ga(2) computed	-0.060	-7.011	7.072	8.131	0.983
La measured	-0.86 ± 0.01	1.65 ± 0.01	-0.80 ± 0.01	1.71 ± 0.01	0.04 ± 0.01
La computed	-0.948	1.907	-0.959	1.907	0.005

powder x-ray diffraction [17]. The lower ^{71}Ga resonance near 2.5 MHz was not obtained due to the limitations of the tuning range of the resonance tank circuit.

2. *Knight Shift and Spin-Lattice Relaxation Rate*

The temperature dependence of the magnetic Knight shift along the b direction, K_{bb}, is shown in Fig. 2(b) for both the ^{139}La and ^{69}Ga(1) sites. The shift is largely temperature-independent up to 100 K, and exhibits a small increase ($\sim 20\%$) between 100-300 K for both sites. The shift arises due to hyperfine couplings between the

nuclear spin and both the orbital and the Pauli spin components of the susceptibility [38]. In general, the shift can be written as: $K = K_o + K_s$, where $K_o = B_D\chi_D$ and $K_s = B_P\chi_P$ are orbital and spin contributions to the shift, and $B_{D,P}$ are the hyperfine coupling constants to these degrees of freedom. In materials where K and χ vary with temperature, it is possible to extract B_P by plotting K versus χ, but the temperature independence of these quantities precludes this approach in this case. It is therefore not straightforward to determine what portion of K_{bb} arises due to orbital versus spin contributions.

Fig. 2(c) displays the temperature dependence of the spin-lattice relaxation rate divided by temperature, $(T_1T)^{-1}$, measured with field along the b direction. There is little to no temperature dependence evident for either site, however the small increase in $(T_1T)^{-1}$ with decreasing temperature could herald the presence of some weak magnetic correlations. There is a small increase in the La relaxation rate near 5 K. This feature is even weaker in the Ga relaxation rate. The relaxation curves also have some evidence for stretched behavior, with stretching exponent $\beta = 0.8$ near this temperature. This behavior suggests that there might be some dilute magnetic impurities present that freeze out, although the bulk susceptibility shows no evidence of a Curie contribution from such impurities [39].

IV. DISCUSSION

Korringa behavior, or temperature-independence of $(T_1T)^{-1}$, is a hallmark of conductors and arises due to spin-flip scattering between the nuclear spins and the spins of the electrons at the Fermi surface [40]. For a single hyperfine coupling channel with an isotropic Fermi-contact type interaction, $T_1TK_s^2 = S_0$ is a temperature independent constant, where $S_0 = (\gamma_e/\gamma_n)^2\hbar/(4\pi k_B)$, and $\gamma_{e,n}$ is the gyromagnetic ratio of the electron/nucleus. Figure 3 displays the Korringa ratio, $T_1TK_{bb}^2/S_0$, for both the ^{139}La and ^{69}Ga(1) sites in $LaNiGa_2$ as a function of temperature, and compares this quantity with several other materials. In principle we should use $K_s = K_{bb} - K_o$ rather than K_{bb}, however we are unable to independently measure K_o. As a result, this discrepancy likely gives rise to the fact that the ratio is different than unity for the ^{69}Ga(1) and ^{139}La sites.

In the presence of exchange enhancements of the conduction electron spin susceptibility, the Korringa ratio can deviate strongly from unity [41, 42]. For the simplified case of a single, spherical Fermi surface, the size of the ratio can be directly related to the Stoner enhancement factor. In this case, a ratio greater than unity heralds ferromagnetic fluctuations, whereas a ratio less than unity indicates antiferromagnetic fluctuations. This trend is evident in Fig. 3 for several other materials known to exhibit either ferromagnetic order or antiferromagnetic fluctuations, including Sr_2RuO_4, which exhibits TRS breaking in the superconducting state [8], UPt_3, which exhibits non-unitary triplet superconductivity [2], and $K_2Cr_3As_3$, which exhibits chiral p-wave superconductivity [26]. Although none of these materials exhibits a single band with a spherical Fermi surface, it is clear that $LaNiGa_2$ is qualitatively different, with a temperature-independent ratio that is fairly close to unity for both the ^{139}La and ^{69}Ga sites.

Further evidence for a lack of correlations is provided by the fact that the measured EFG values are relatively close to those computed by the DFT band structure. In materials that exhibit strong correlations, the measured EFGs can differ significantly from those computed via band structure [43, 44]. The calculations used here for $LaNiGa_2$ did not include any Coulomb repulsion terms, but still are within 20% with the measured values. This fact suggests that correlations are relatively small in this material.

In summary, we find that $LaNiGa_2$ does not exhibit any significant Stoner enhancement but only weak spin fluctuations. The unusual superconducting state with an imbalance between equal-spin pairing gaps most likely does not arise from large electronic interactions that are believed to drive unconventional superconductivity in many strongly correlated systems. The topological band structure, with degenerate bands at the Fermi level, can enable equal-spin pairing gaps, as described in Ref. [14, 17]. The role of topology to induce TRS breaking in $LaNiGa_2$ remains an open theoretical question. An alternative explanation for the TRS breaking observed in μSR could be that there is conventional spin-singlet pairing with another nearly degenerate superconducting state, resulting in complex combinations of superconducting states being stabilized near impurities [45], or local defects such as grain boundaries or vacancies could affect the phase factors of the multiple gap functions leading to spontaneous current patterns [46]. Our results motivate revisiting μSR studies on single crystals to better understand the TRS breaking. Future NMR experiments below T_c may shed light on the nature of the unusual pairing gaps in this system.

Acknowledgment. We acknowledge helpful discussions with W. Pickett and F. Ronning. Work at UC Davis was supported by the NSF under Grant No. DMR-2210613 and by the UC Laboratory Fees Research Program (LFR-20-653926). NQR measurements at LANL were performed with support from the UC Fees Research Program. ASB and MCY were supported by the NSF under Grant No. DMR-2323971. The XPS work was supported by the Alfred P.Sloan Foundation (FG-2019-12170) and the Dean's Faculty Fellowship at the College of Letters and Sciences at UC Davis.

Appendix A: XPS

Fig. A1 displays a series of Ga $2p_{3/2}$ core level spectra under different conditions with different degrees of surface versus bulk sensitivity. The spectra were then

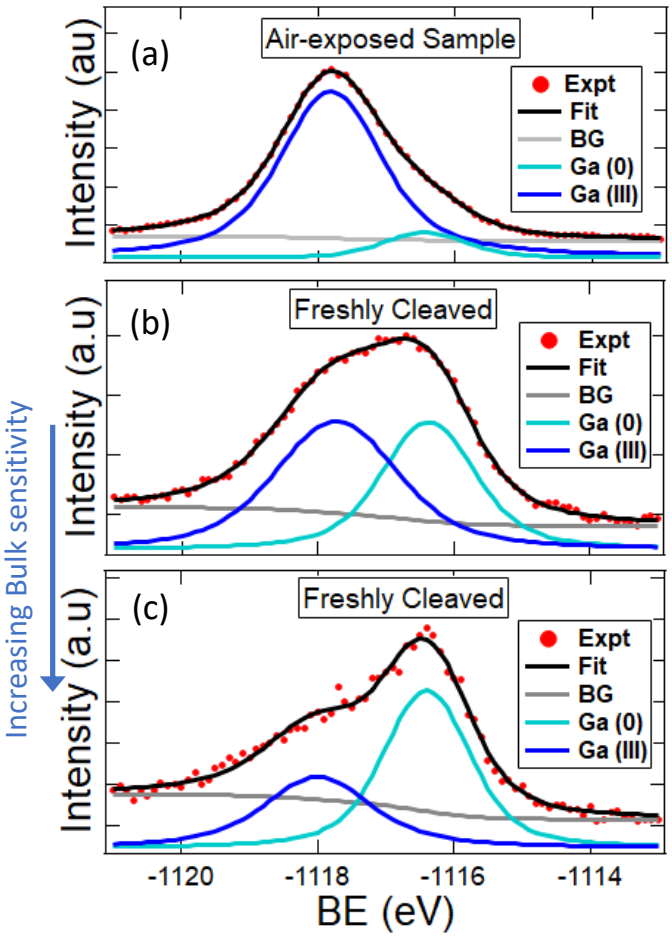

FIG. A1. Fig 1: X-ray Photoemission Spectroscopy of Ga-$2p_{3/2}$ in $LaNiGa_2$. (a) Air-exposed spectrum; (b) Spectrum of the same sample cleaved ex-situ before measurement; and (c) Spectrum of the sample as in (b) but with Ag L-α source.

fit with a Shirley background [47] and two Voigt lineshapes each corresponding to surface and bulk species. The binding energies across data sets (air-exposed vs freshly cleaved vs Ag source) were kept consistent. The binding energies were calibrated to a reference gold $4f$ spectrum. The Lorentzian width and Gaussian widths of the gold reference were found to be 0.385 eV and 0.339 eV, respectively.

Appendix B: NMR

In a magnetic field, the La spectrum is split into seven resonances as shown in Fig. B1. The Ga, on the other hand, is split into three resonances for each site, as shown for ^{69}Ga for field along the b-axis in Fig. B2(a). This spectrum shows two sets of quadrupolar satellites, and narrow overlapping central resonances. To better determine the EFG tensor elements, we measured the spectrum as a function of field orientation in the ac plane, as shown in Fig. B2(b) for the central transition. There are three resonances visible, and their angular dependence is shown in Fig. B3. Two of the peaks have roughly equal intensity, and there is a third peak at lower frequency with slightly lower intensity. The origin of this third peak is unknown, and we do not observe any associated quadrupolar satellite peaks. The angular dependence of the central and satellite peaks were globally fit for each site using perturbation theory to extract the EFG tensor elements, ν_{aa} and ν_{cc} in Eq. 1, and the fitted values are given in Table II.

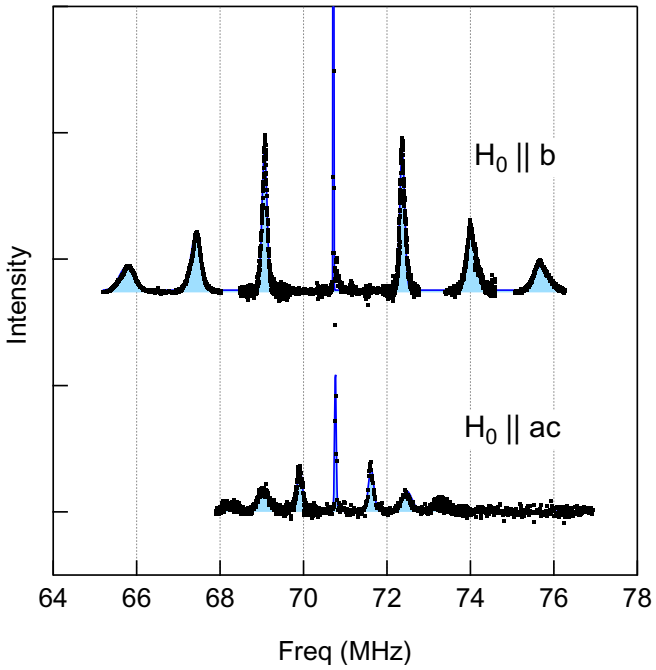

FIG. B1. ^{139}La NMR spectra in $LaNiGa_2$ in an external magnetic field of $\mu_0 H_0 = 11.7286$ T at 5 K for fields parallel and perpendicular to b. The filled regions show a fit to the spectra to an exact diagonalization of Eq. 1.

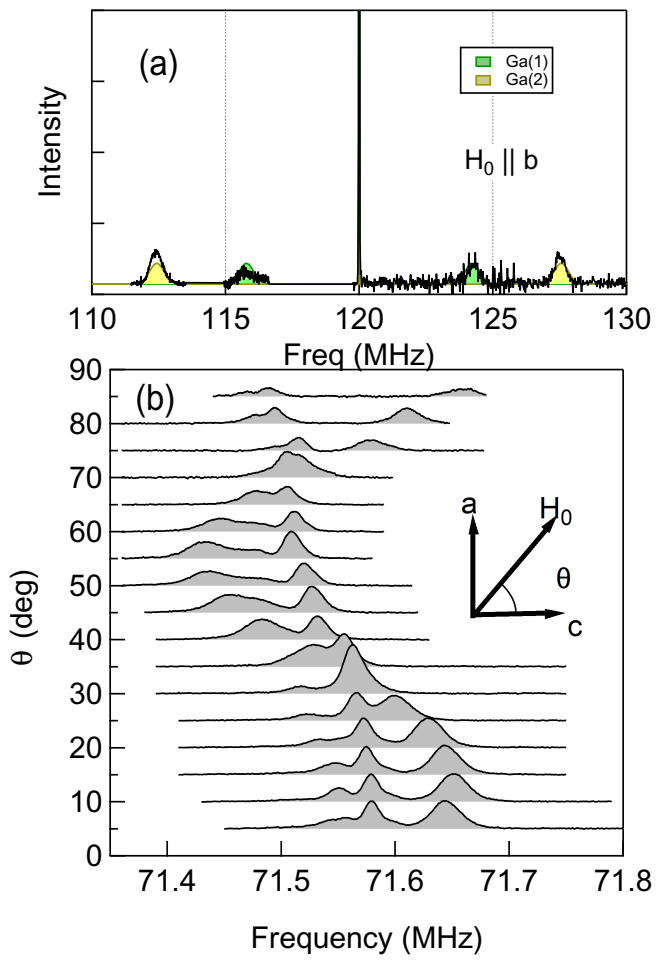

FIG. B2. (a) ^{69}Ga spectrum in $LaNiGa_2$ for $\mathbf{H}_0 \parallel b$ for $\mu_0 H_0 = 11.7286$ T at 2.7 K. The filled regions show fits to the spectra to an exact diagonalization of Eq. 1. (b) Central transition of ^{69}Ga as a function of field orientation in the ac-plane, where the angle, θ, is measured relative to the c-axis, at 7.0 T and 2.7 K.

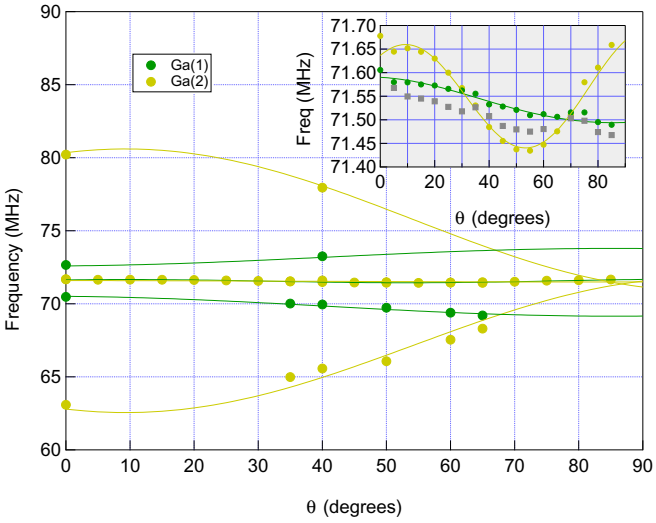

FIG. B3. Angular dependence of the ^{69}Ga resonances as a function of θ. The solid lines are fits as described in the text. The inset focuses on the central transition alone.

[1] P. Monthoux, D. Pines, and G. G. Lonzarich, Superconductivity without phonons, Nature **450**, 1177 (2007).

[2] H. Tou, Y. Kitaoka, K. Ishida, K. Asayama, N. Kimura, Y. Ōnuki, E. Yamamoto, Y. Haga, and K. Maezawa, Nonunitary spin-triplet superconductivity in UPt_3: Evidence from ^{195}Pt Knight shift study, Phys. Rev. Lett. **80**, 3129 (1998).

[3] V. P. Mineev and K. V. Samokhin, *Introduction to unconventional superconductivity* (Gordon and Breach Science Publishers, Amsterdam, The Netherlands, 1999).

[4] H. Q. Yuan, D. F. Agterberg, N. Hayashi, P. Badica, D. Vandervelde, K. Togano, M. Sigrist, and M. B. Salamon, s-wave spin-triplet order in superconductors without inversion symmetry: Li_2Pd_3B and Li_2Pt_3B, Phys. Rev. Lett. **97**, 017006 (2006).

[5] C. Kallin and J. Berlinsky, Chiral superconductors, Rep. Prog. Phys. **79**, 054502 (2016).

[6] M. Sato and Y. Ando, Topological superconductors: a review, Rep. Prog. Phys. **80**, 076501 (2017).

[7] C. Nayak, S. H. Simon, A. Stern, M. Freedman, and S. Das Sarma, Non-abelian anyons and topological quantum computation, Rev. Mod. Phys. **80**, 1083 (2008).

[8] G. M. Luke, Y. Fudamoto, K. M. Kojima, M. I. Larkin, J. Merrin, B. Nachumi, Y. J. Uemura, Y. Maeno, Z. Q. Mao, Y. Mori, H. Nakamura, and M. Sigrist, Time-reversal symmetry-breaking superconductivity in Sr_2RuO_4, Nature **394**, 558 (1998).

[9] B. M. Huddart, I. J. Onuorah, M. M. Isah, P. Bonfà, S. J. Blundell, S. J. Clark, R. De Renzi, and T. Lancaster, Intrinsic nature of spontaneous magnetic fields in superconductors with time-reversal symmetry breaking, Phys. Rev. Lett. **127**, 237002 (2021).

[10] J. Xia, Y. Maeno, P. T. Beyersdorf, M. M. Fejer, and A. Kapitulnik, High resolution polar Kerr effect measurements of Sr_2RuO_4: Evidence for broken time-reversal symmetry in the superconducting state, Phys. Rev. Lett. **97**, 167002 (2006).

[11] A. D. Hillier, J. Quintanilla, B. Mazidian, J. F. Annett, and R. Cywinski, Nonunitary triplet pairing in the centrosymmetric superconductor $LaNiGa_2$, Phys. Rev. Lett. **109**, 097001 (2012).

[12] A. D. Hillier, J. Quintanilla, and R. Cywinski, Evidence for time-reversal symmetry breaking in the noncentrosymmetric superconductor $LaNiC_2$, Phys. Rev. Lett. **102**, 117007 (2009).

[13] L. P. Gor'kov and E. I. Rashba, Superconducting 2D system with lifted spin degeneracy: Mixed singlet-triplet state, Phys. Rev. Lett. **87**, 037004 (2001).

[14] Z. F. Weng, J. L. Zhang, M. Smidman, T. Shang, J. Quintanilla, J. F. Annett, M. Nicklas, G. M. Pang, L. Jiao, W. B. Jiang, Y. Chen, F. Steglich, and H. Q. Yuan, Two-gap superconductivity in $LaNiGa_2$ with nonunitary triplet pairing and even parity gap symmetry, Phys. Rev. Lett. **117**, 027001 (2016).

[15] S. K. Ghosh, G. Csire, P. Whittlesea, J. F. Annett, M. Gradhand, B. Újfalussy, and J. Quintanilla, Quantitative theory of triplet pairing in the unconventional superconductor $LaNiGa_2$, Phys. Rev. B **101**, 100506 (2020).

[16] S. Sundar, M. Yakovlev, N. Azari, M. Abedi, D. M. Broun, H. U. Ozdemir, S. R. Dunsiger, D. Zackaria, V. Taufour, and J. E. Sonier, Gap structure of the noncentrosymmorphic superconductor $LaNiGa_2$ probed by muSR, (2023), arXiv:2311.00069 [cond-mat.supr-con].

[17] J. R. Badger, Y. Quan, M. C. Staab, S. Sumita, A. Rossi, K. P. Devlin, K. Neubauer, D. S. Shulman, J. C. Fettinger, P. Klavins, S. M. Kauzlarich, D. Aoki, I. M. Vishik, W. E. Pickett, and V. Taufour, Dirac lines and loop at the Fermi level in the time-reversal symmetry breaking superconductor $LaNiGa_2$, Communications Physics **5**, 22 (2022).

[18] T. M. R. Wolf, M. F. Holst, M. Sigrist, and J. L. Lado, Nonunitary multiorbital superconductivity from competing interactions in Dirac materials, Phys. Rev. Res. **4**, L012036 (2022).

[19] N. Curro, T. Caldwell, E. Bauer, L. Morales, M. Graf, Y. Bang, A. Balatsky, J. Thompson, and J. Sarrao, Unconventional superconductivity in $PuCoGa_5$, Nature **434**, 622 (2005).

[20] P. Blaha, K. Schwarz, F. Tran, R. Laskowski, G. K. H. Madsen, and L. D. Marks, WIEN2k: An APW+lo program for calculating the properties of solids, J. Chem. Phys. **152**, 074101 (2020).

[21] J. P. Perdew, K. Burke, and M. Ernzerhof, Generalized gradient approximation made simple, Phys. Rev. Lett. **77**, 3865 (1996).

[22] P. Jeglič, A. Potočnik, M. Klanjšek, M. Bobnar, M. Jagodič, K. Koch, H. Rosner, S. Margadonna, B. Lv, A. M. Guloy, and D. Arčon, ^{75}As nuclear magnetic resonance study of antiferromagnetic fluctuations in the normal state of LiFeAs, Phys. Rev. B **81**, 140511 (2010).

[23] Y. Tokunaga, H. Sakai, S. Kambe, T. Hattori, N. Higa, G. Nakamine, S. Kitagawa, K. Ishida, A. Nakamura, Y. Shimizu, Y. Homma, D. Li, F. Honda, and D. Aoki, ^{125}Te-NMR study on a single crystal of heavy fermion superconductor UTe_2, J. Phys. Soc. Jpn. **88**, 073701 (2019).

[24] K. Ishida, D. Ozaki, T. Kamatsuka, H. Tou, M. Kyogaku, Y. Kitaoka, N. Tateiwa, N. K. Sato, N. Aso, C. Geibel, and F. Steglich, Spin-triplet superconductivity in UNi_2Al_3 revealed by the ^{27}Al Knight shift measurement, Phys. Rev. Lett. **89**, 037002 (2002).

[25] K. Rana, H. Kotegawa, R. R. Ullah, J. S. Harvey, S. L. Bud'ko, P. C. Canfield, H. Tou, V. Taufour, and Y. Furukawa, Magnetic fluctuations in the itinerant ferromagnet $LaCrGe_3$ studied by ^{139}La NMR, Phys. Rev. B **99**, 214417 (2019).

[26] J. Yang, J. Luo, C. Yi, Y. Shi, Y. Zhou, and G. qing Zheng, Spin-triplet superconductivity in $K_2Cr_3As_3$, Sci. Adv. **7**, eabl4432 (2021).

[27] M. Lee, G. F. Moores, Y.-Q. Song, W. P. Halperin, W. W. Kim, and G. R. Stewart, ^{195}Pt spin dynamics and Knight shift in single crystals of UPt_3, Phys. Rev. B **48**, 7392 (1993).

[28] T. Imai, A. Hunt, K. Thurber, and F. Chou, ^{17}O NMR evidence for orbital dependent ferromagnetic correlations in Sr_2RuO_4, Phys. Rev. Lett. **81**, 3006 (1998).

[29] Y. Quan, V. Taufour, and W. E. Pickett, Nonsymmorphic band sticking in a topological superconductor, Phys. Rev. B **105**, 064517 (2022).

[30] L. B. Mendelsohn, F. Biggs, and J. B. Mann, Hartree-Fock diamagnetic susceptibilities, Physical Review A **2**, 1130 (1970).

[31] G. A. Bain and J. F. Berry, Diamagnetic corrections and Pascal's constants, Journal of Chemical Education **85**, 532 (2008).

[32] G. Schön, Auger and direct electron spectra in X-ray photoelectron studies of zinc, zinc oxide, gallium and gallium oxide, J. Electron Spectrosc. **2**, 75 (1973).

[33] C. D. Wagner, Chemical shifts of Auger lines, and the Auger parameter, Faraday Discuss. Chem. Soc. **60**, 291 (1975).

[34] M. P. Seah and W. A. Dench, Quantitative electron spectroscopy of surfaces: A standard data base for electron inelastic mean free paths in solids, Surface and Interface Analysis **1**, 2 (1979).

[35] C. Kittel, *Introduction to Solid State Physics*, 8th ed. (Wiley, 2004).

[36] Y. Iwamoto, Y. Iwasaki, K. Ueda, and T. Kohara, Microscopic measurements in ^{139}La-NQR of the ternary carbide superconductor $LaNiC_2$, Phys. Lett. A **250**, 439 (1998).

[37] J. Hwang, P. Canepa, and T. Scott, Pressure dependence of the electric field gradient and knight shift tensors of single crystal gallium, J. Phys. Chem. Solids **38**, 1403 (1977).

[38] C. P. Slichter, *Principles of Nuclear Magnetic Resonance*, 3rd ed. (Springer-Verlag, 1992).

[39] M. Frachet, I. Vinograd, R. Zhou, S. Benhabib, S. Wu, H. Mayaffre, S. Krämer, S. K. Ramakrishna, A. P. Reyes, J. Debray, T. Kurosawa, N. Momono, M. Oda, S. Komiya, S. Ono, M. Horio, J. Chang, C. Proust, D. LeBoeuf, and M.-H. Julien, Hidden magnetism at the pseudogap critical point of a cuprate superconductor, Nat. Phys. **16**, 1064 (2020).

[40] J. Korringa, Nuclear magnetic relaxation and resonnance line shift in metals, Physica **16**, 601 (1950).

[41] T. Moriya, The effect of electron-electron interaction on the nuclear spin relaxation in metals, J. Phys. Soc. Jpn. **18**, 516 (1963).

[42] A. Narath and H. T. Weaver, Effects of electron-electron interactions on nuclear spin-lattice relaxation rates and Knight shifts in alkali and noble metals, Phys. Rev. **175**, 373 (1968).

[43] E. P. Stoll, P. F. Meier, and T. A. Claxton, Electric field gradients from first-principles and point-ion calculations, Phys. Rev. B **65**, 064532 (2002).

[44] S. Jalali Asadabadi, Electronic structure and electric-field gradient analysis in $CeIn_3$, Phys. Rev. B **75**, 205130 (2007).

[45] B. M. Andersen, A. Kreisel, and P. J. Hirschfeld, Spontaneous time-reversal symmetry breaking by disorder in superconductors (2023), arXiv:2312.08099 [cond-mat.supr-con].

[46] V. Stanev and Z. Tešanović, Three-band superconductivity and the order parameter that breaks time-reversal symmetry, Phys. Rev. B **81**, 134522 (2010).

[47] D. A. Shirley, High-resolution X-ray photoemission spectrum of the valence bands of gold, Phys. Rev. B **5**, 4709 (1972).